

21-cm absorption from galaxies at $z \sim 0.3$

N. Gupta^{1,2}, R. Srianand², P. Noterdaeme³, P. Petitjean³, and S. Muzahid²

¹ ASTRON, the Netherlands Institute for Radio Astronomy, Postbus 2, 7990 AA, Dwingeloo, The Netherlands
e-mail: gupta@astron.nl

² IUCAA, Post Bag 4, Ganeshkhind, Pune 411007, India

³ UPMC-CNRS, UMR7095, Institut d'Astrophysique de Paris, F-75014 Paris, France

Received 30 Mar 2013; Accepted 16 Aug 2013

ABSTRACT

We report the detection of 21-cm absorption from foreground galaxies towards quasars, specifically $z_{\text{gal}}=0.3120$ towards SDSS J084957.97+510829.0 ($z_{\text{qso}}=0.584$; Pair-I) and $z_{\text{gal}}=0.3714$ towards SDSS J144304.53+021419.3 ($z_{\text{qso}}=1.82$; Pair-II). In both the cases, the integrated 21-cm optical depth is consistent with the absorbing gas being a damped Lyman- α (DLA) system. In the case of Pair-I, strong Na I and Ca II absorption lines are also detected at z_{gal} in the QSO spectrum. We identify an early-type galaxy at an impact parameter of $b \sim 14$ kpc whose photometric redshift is consistent with that of the detected metal and 21-cm absorption lines. This would be the first example of an early-type galaxy associated with an intervening 21-cm absorber. The gas detected in 21-cm and metal absorption lines on the outskirts of this luminous red galaxy could be associated with the reservoir of cold H I gas with a low level of star formation activity in the outer regions of the galaxy as reported in the literature for $z \sim 0.1$ early-type galaxies. In the case of Pair-II, the absorption is associated with a low surface brightness galaxy that, unlike most other known quasar-galaxy pairs (QGPs), i.e. QSO sight lines passing through disks or halos of foreground galaxies, is identified only via narrow optical emission lines detected on top of the QSO spectra. Using SDSS spectra we infer that the emission lines originate within ~ 5 kpc of the QSO sight line, and the gas has metallicity $[12+\text{O}/\text{H}] \sim 8.4$ and star formation rate $\sim 0.7\text{--}0.8 M_{\odot} \text{ yr}^{-1}$. The measured 21-cm optical depth can be reconciled with the $N(\text{H I})$ we derive from the measured extinction ($A_V=0.6$) if either the H I gas is warm or the extinction per hydrogen atom in this galaxy is much higher than the mean value of the Small Magellanic Cloud. Finally, using a sample of 9 QGPs with 21-cm absorption detection from our observations and literature, we report a weak anti-correlation (Spearman rank, $r_s=-0.3$) between the 21-cm optical depth and galaxy impact parameter. Milliarcsecond scale images and spectra are required to understand the implications of this.

Key words. quasars: absorption lines – galaxies: evolution – galaxies: ISM – galaxies: star formation.

1. Introduction

It is well known that physical conditions in the diffuse interstellar medium (ISM) of galaxies are influenced by various radiative and mechanical feedback processes associated with in-situ star formation (e.g., Wolfire et al. 2003). Therefore, volume-filling factors of different phases of gas in a galaxy are expected to depend on its star formation history. Of particular interest is the evolution of the volume-filling factor of cold neutral medium (CNM) phase that also serves as a gaseous reservoir for star formation in galaxies. It is expected to contain an imprint of the collective outcome of all the processes that shape the star formation history of the Universe (e.g., Hopkins & Beacom 2006). Systematic searches of high- z *intervening* 21-cm absorbers in samples of Mg II systems and damped Ly α systems (DLAs) towards QSOs to measure CNM filling factor of galaxies have resulted in detections of 21-cm absorption towards $\sim 10\text{--}20\%$ of Mg II systems (e.g., Briggs & Wolfe 1983; Lane 2000; Gupta et al. 2009; Kanekar et al. 2009; Gupta et al. 2012) and DLAs (e.g., Kanekar & Chengalur 2003; Curran et al. 2010; Srianand et al. 2012). However, establishing a connection between the redshift evolution of 21-cm absorbers and global star formation rate density is not straight forward due to (i) small number statistics of 21-cm absorbers, (ii) ambiguities regarding the origin of absorbing gas (i.e., gaseous disk, halo or outflowing/infalling gas etc.)

and (iii) issues related to the small scale structure in absorbing gas and the extent of radio source.

Blind searches of 21-cm absorption with Square Kilometre Array (SKA) pathfinders in the near future are expected to significantly increase the number of intervening 21-cm absorbers over a wide redshift range. To understand the nature of absorbers detected from these, it is important to establish a link between the properties of galaxies and intervening 21-cm absorbers, and address issues related to points (ii) and (iii) mentioned above. At present, both these points are best addressed at $z \lesssim 0.2$ where it is possible to determine properties of absorbing gas on pc and kpc scales via arcsecond and milliarcsecond scale spectroscopy, and detect the galaxy responsible for absorption in 21-cm and various optical emission lines. However, almost all the intervening 21-cm absorption line searches until now have happened at $z \gtrsim 0.2$. The notable exceptions in the recent past are Gupta et al. (2010), Borthakur et al. (2011), and Darling et al. (2011) (see also Carilli & van Gorkom 1992). The first two are based on samples of QSO sight lines passing through disks or halos of foreground galaxies, which we henceforth refer to as quasar-galaxy pairs (QGPs), whereas the last is a blind search for 21-cm absorption at $z \lesssim 0.06$ using the Arecibo telescope. All three have detected one 21-cm absorber each and showcase difficulties in detecting 21-cm absorbers at low- z in the absence of large catalogs of Mg II systems and DLAs.

To move forward, we are systematically searching the Sloan Digital Sky Survey (SDSS) for QGPs with angular separation $<10''$ and background quasar flux density $\gtrsim 100$ mJy in the Faint Images of the Radio Sky at Twenty-Centimeters (FIRST) catalog. The objective is to search for 21-cm absorption in QGPs with impact parameter <30 kpc and systematically increase the number of low- z intervening 21-cm absorbers/DLAs. This sample of low- z absorbers can then be used as a comparison sample to understand the nature of high- z 21-cm absorbers and DLAs (see Krogager et al. 2012 and references therein for the current status of $z > 2$ DLA host galaxies). In this paper, we report the detection of 21-cm absorption from two foreground galaxies at $z_{\text{gal}} \sim 0.3$ towards quasars SDSS J084957.97+510829.0 ($z_{\text{qso}}=0.584$, hereafter J0849+5108) and SDSS J144304.53+021419.3 ($z_{\text{qso}}=1.82$, hereafter J1443+0214). These two pairs with foreground galaxies at $z_{\text{gal}} \sim 0.3$ were identified while scanning the SDSS images and spectra of bright radio sources and are interesting in their own right. In both these cases, the measured 21-cm optical depth is consistent with the absorbing gas being a DLA. The nature of background radio source in the case of QGP J0849+5108 has been the subject of considerable debates and is suspected of being affected by foreground galaxy lensing. The quasar sight line is positioned close to a pair of low- z ($z_{\text{gal}} \sim 0.07$) interacting spiral galaxies, and the field contains many bright galaxies within $60''$ of the quasar (Stickel et al. 1989). The sight line has been previously searched for 21-cm and molecular absorption lines (Boisse et al. 1988; Wiklind & Combes 1995; Gupta et al. 2010).

The QGP J1443+0214 differs in the way it has been identified. Unlike most other QGPs studied to date, this QGP is identified by the novel technique of detecting emission lines from a foreground galaxy in the spectra of QSOs (see e.g., Noterdaeme et al. 2010b; York et al. 2012). The foreground galaxy is otherwise invisible in this case. In Section 2, we present details of our observations. We then detail the properties of individual QGPs in Section 3. In Section 4, we discuss implications of our results. Throughout this paper we use the Λ CDM cosmology with $\Omega_m=0.27$, $\Omega_\Lambda=0.73$, and $H_0=71 \text{ km s}^{-1} \text{ Mpc}^{-1}$.

2. Radio observations

Both the pairs were observed with Giant Metrewave Radio Telescope (GMRT) using a baseband bandwidth of 4.17 MHz split into 512 spectral channels (resolution $\sim 2.3 \text{ km s}^{-1}$) centered on the redshifted 21-cm frequency of foreground galaxies. The QGP J0849+5108 was observed on 2011 July 18 (2.7 hrs on source) and J1443+0214 on 2012 June 2 (5.7 hrs on source). Standard calibrators were regularly observed during the observations for flux density, bandpass, and phase calibrations. The data were reduced using the Astronomical Image Processing System (AIPS) following standard procedures as in Gupta et al. (2010). Both the quasars are represented well by a single Gaussian component, i.e. unresolved in our GMRT images that have spatial resolution of $\sim 4'' \times 3''$. The flux densities of J0849+5108 and J1443+0214 were measured to be 245 mJy and 163 mJy, and spectral rms to be $\sim 2.0 \text{ mJy beam}^{-1} \text{ channel}^{-1}$ and $\sim 0.9 \text{ mJy beam}^{-1} \text{ channel}^{-1}$, respectively. In both cases, we detected 21-cm absorption consistent with the redshift of the foreground galaxy. In the case of J0849+5108, a few frequency channels on either side of the detected absorption feature were found to be affected by RFI (see shaded regions in Fig. 1). We therefore reobserved this QGP on 2012 July 3 (3.5 hrs on source) to confirm the absorption. The flux density of the quasar was mea-

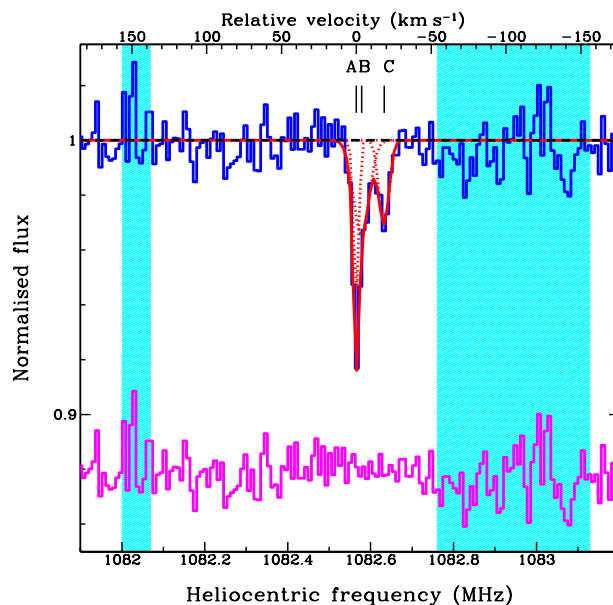


Fig. 1. The 21-cm absorption detected towards the QGP J0849+5108. Origin of the velocity scale given at the top is defined with respect to the maximum of optical depth. Individual Gaussian components labelled as A, B, and C (see Table 1) and resulting fits to the absorption profile are plotted as dotted and continuous lines, respectively. Residuals are also shown with an arbitrary flux offset for clarity. Shaded regions mark the frequency range affected by RFI.

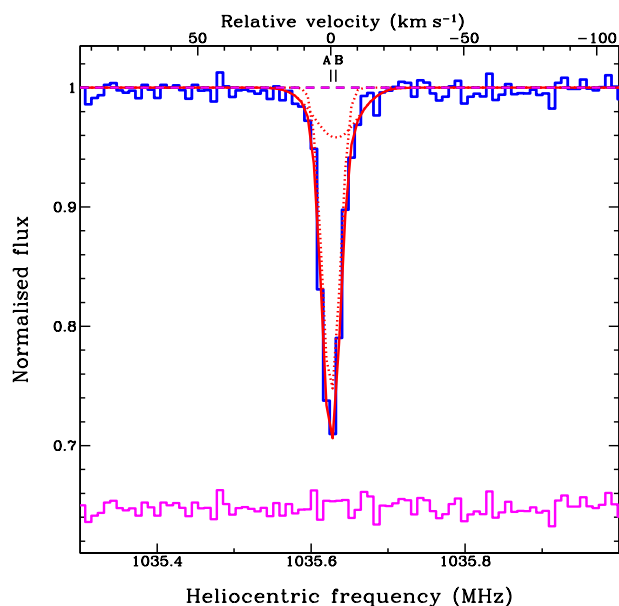


Fig. 2. The 21-cm absorption detected towards J1443+0214. The other details are same as in Fig. 1.

sured to be 221 mJy, i.e. $\sim 10\%$ lower than the value measured in the first observing run. The velocity shift due to heliocentric motion of the Earth between the two observing runs on this QGP is 5.6 km s^{-1} . The repeat observation reproduced the previously detected absorption feature at the expected frequency. This confirms the reality of the absorption. The spectrum presented in Fig. 1 is obtained by the inverse-rms-square weighted average of the *normalized* spectra obtained from two observing runs. The 21-cm absorption spectrum towards J1443+0214 is presented in Fig. 2.

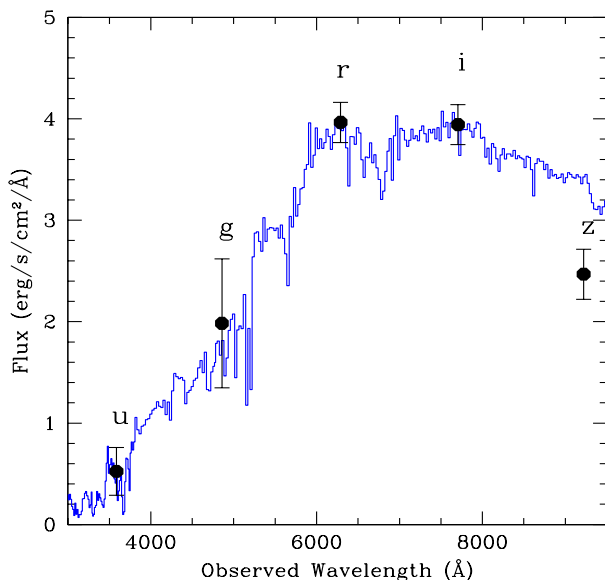


Fig. 3. SDSS photometric points of the galaxy J084958.09+510826.7 overlaid on a typical luminous red galaxy spectrum at $z_{\text{gal}}=0.3120$.

In the case of absorber towards J0849+5108, the total integrated 21-cm optical depth, $\int \tau dv = 0.95 \pm 0.06 \text{ km s}^{-1}$. Overall, 90% of the total optical depth is contained within 22.5 km s^{-1} . In the case of J1443+0214, the total integrated 21-cm optical depth is $3.4 \pm 0.1 \text{ km s}^{-1}$, and 90% of the total optical depth is contained within 16.5 km s^{-1} . We parametrize both the absorption profiles using multiple Gaussian components. The fits are shown in Figs. 1 and 2, and details of Gaussian components are provided in Table 1.

Table 1. Multiple Gaussian fits to the 21-cm absorption profiles. Listed are the component identification and corresponding redshift, full width at half maximum (FWHM), and peak optical depth.

Quasar	ID	z_{abs}	FWHM (km s^{-1})	τ_{peak}
J0849+5108	A	0.312074	4 ± 1	0.059 ± 0.010
	B	0.312058	13 ± 2	0.035 ± 0.008
	C	0.311992	8 ± 2	0.031 ± 0.004
J1443+0214	A	0.371544	8 ± 1	0.297 ± 0.017
	B	0.371535	19 ± 4	0.043 ± 0.015

3. Physical properties in individual cases

3.1. $z_{\text{gal}} = 0.3120$ galaxy towards J0849+5108

The background radio source in this case is a well-known object that has a BL Lacertae-like spectrum during outbursts (Arp et al. 1979). The nature of this object has been the subject of considerable debate. There are speculations about its optical spectrum being affected by foreground galaxy lensing and/or reddening (Stickel et al. 1989; Östman et al. 2006). Interestingly, there are two foreground galaxies at angular separation less than $15''$ to the radio source (see Fig. 7 of Gupta et al. 2010), and the sight line has been previously searched for 21-cm and molecular absorption (Boisse et al. 1988; Wiklind & Combes 1995). The galaxy J084957.48+510842.3 ($z_{\text{gal}}=0.073$) situated at $\sim 14''$

($b \sim 19 \text{ kpc}$) north of the radio source is a member of an interacting pair of galaxies (Stickel et al. 1989). No 21-cm absorption was detected from this galaxy by Boisse et al. (1988). The 3σ 21-cm optical depth limit, $\int \tau_{3\sigma} dv$, was 0.32 km s^{-1} . A deeper 21-cm absorption optical depth limit, $\int \tau_{3\sigma} dv = 0.08 \text{ km s}^{-1}$, was obtained for this galaxy using GMRT by Gupta et al. (2010). They also reported the detection of Na I and Ca II absorption at $z_{\text{gal}} = 0.3120$ in the spectrum of the QSO and associated it to a luminous red galaxy (LRG), identified as ‘G1’ in their Fig. 7, at an angular separation of $2.3''$ ($b \sim 14 \text{ kpc}$) southeast of the QSO. While the spectrum of this galaxy is not available in the SDSS catalog, Fig. 3 shows that the SDSS photometry is consistent with an LRG at the absorber’s redshift. Here, we report the detection of 21-cm absorption at the redshift of Na I and Ca II absorption lines (see Fig. 1). The 21-cm absorption profile is well fitted with three Gaussian components presented in Table 1. In principle, the width of 21-cm absorption line can be used to constrain the kinetic temperature, $T_K \leq 21.86 \times \text{FWHM}^2$, of absorbing gas (e.g., Heiles & Troland 2003). For J0849+5108, the FWHM of the strongest and narrowest Gaussian component ‘A’ implies kinetic temperature, $T_K < 350 \text{ K}$.

The observed equivalent widths of Na I absorption lines correspond to $N(\text{Na I}) \geq (6 \pm 2) \times 10^{12} \text{ cm}^{-2}$, assuming the optically thin case. Consequently, we derive $\log N(\text{H I}) \geq 21.2 \pm 0.5$ following the relation

$$\log \frac{N(\text{Na I})}{N(\text{H I})} = -(0.16 \pm 0.06) [\log N(\text{H I}) - 19.5] - (8.12 \pm 0.79) \quad (1)$$

from the known correlation between $N(\text{H I})$ and $N(\text{Na I})$ found in our Galaxy (Ferlet et al. 1985; Wakker & Mathis 2000). By assuming an optically thin cloud with spin temperature T_s and covering factor f_c , the total integrated 21-cm optical depth estimated from the GMRT spectrum corresponds to the H I column density, $N(\text{H I}) = 1.7 \times 10^{20} (T_s/100) (1.0/f_c) \text{ cm}^{-2}$. Therefore, if the absorber was to follow the $N(\text{H I})$ - $N(\text{Na I})$ relation seen in our galaxy, the harmonic mean spin temperature $T_s > 890_{-580}^{+1560} \text{ K}$. Since such high T_s values are typically seen in high- z DLAs (Kanekar & Chengalur 2003; Srianand et al. 2012), it will be important to have a direct Ly α measurement of $N(\text{H I})$ for this system.

The extent of gas detected in absorption is determined by the size of the background source. At milliarcsecond (mas) scales, J0849+5108 exhibits a core-jet morphology with an overall separation of $\sim 4 \text{ mas}$, i.e. $\sim 20 \text{ pc}$ at the z_{gal} (D’Ammando et al. 2012). The 5 GHz Very Long Baseline Array (VLBA) observations simultaneous with the Very Large Array (VLA) observations recover 75% to 85% of the total arcsecond scale flux (see Tables 6 and 7 of D’Ammando et al. 2012). The remaining flux originates in structures on scales $> 40 \text{ mas}$ (i.e., 200 pc at z_{gal}). This suggests that the region probed in the GMRT spectrum probably corresponds to scales $< 20 \text{ pc}$. If the extent of the absorbing gas is $> 20 \text{ pc}$ then this would imply $f_c > 0.7$. Actually, the ‘core’ component is unresolved with size $< 0.3 \text{ mas}$ (i.e., 1.4 pc at $z_{\text{gal}}=0.3120$) and contains about 95% of the total mas-scale flux at 5-10 GHz. Thus, the derived constraints on f_c and extent of the region probed in 21-cm absorption are conservative.

As previously mentioned, while J0849+5108 has a spectral energy distribution (SED) similar to that of a blazar, Yuan et al. (2008) identified it as a radio-bright narrow-line Seyfert 1 AGN with an additional contribution to the optical flux coming from a mildly relativistic jet. The intrinsic spectrum is uncertain and most likely very different from the median QSO spectrum of

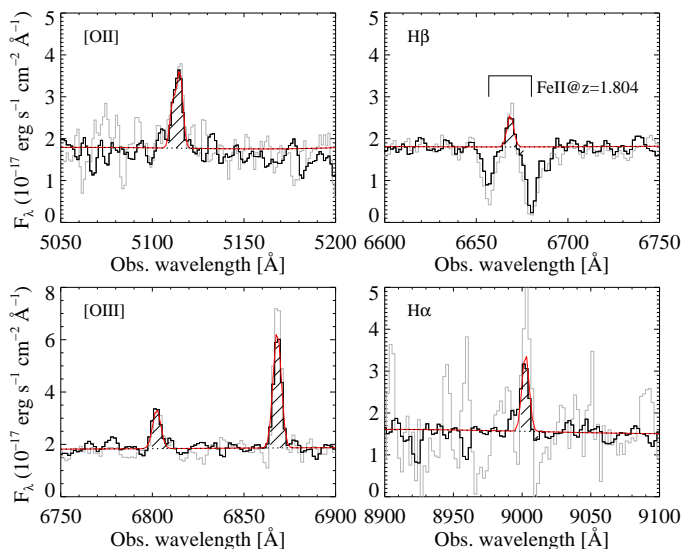


Fig. 4. Fit to the galactic emission lines at $z_{\text{gal}} = 0.3714$ towards J1443+0214. The DR9 spectrum is shown in black, and the 3-pixel boxcar-smoothed DR7 spectrum is shown in gray. The absorption lines seen on each side of $H\beta$ are due to $\text{Fe II } \lambda\lambda 2344, 2374$ at $z_{\text{abs}} = 1.804$.

Vanden Berk et al. (2001). Therefore, unlike the case of QGP J1443+0214 discussed next, it is not possible to obtain an independent estimate of $N(\text{H I})$ by SED fitting in this case.

3.2. $z_{\text{gal}}=0.3714$ galaxy towards J1443+0214

Unlike most QGPs studied until now, where one clearly identifies a foreground galaxy in optical images, the galaxy in the case of QGP J1443+0214 is identified by the detection of emission lines in the SDSS spectrum of QSO. The foreground galaxy is invisible otherwise. The SDSS spectrum [both in SDSS-II (DR7) and SDSS-III (DR9)] of QSO J1443+0214 shows broad emission lines at $z_{\text{em}} = 1.82$ and a set of narrow emission lines (i.e., [O II], [O III], $H\beta$, and $H\alpha$) at $z_{\text{gal}}=0.3714$ (see Fig. 4) like the foreground galaxies detected by Noterdaeme et al. (2010b) in the SDSS spectra of high- z QSOs. We do not detect any significant difference in the line strengths between the SDSS-II (DR7) and SDSS-III (DR9) spectra, while the fiber diameters are of $3''$ (15 kpc at z_{gal}) and $2''$ (10 kpc at z_{gal}), respectively. Therefore the line emission probably originates in a low surface brightness region within 5 kpc to the QSO sight line. This is also confirmed by the non-detection of the galaxy in SDSS images after subtracting the QSO contribution and by the fact that the SED fitting as in Fig. 5 (see below) did not require any additional contribution from the galaxy continuum.

We estimated the color excess $E(B-V)$ by fitting the SDSS-II SED of QSO J1443+0214 by the SDSS-II QSO composite from Vanden Berk et al. (2001). The $<2000 \text{ \AA}$ rest-wavelength coverage for the composite spectrum was taken from Telfer et al. (2002). We reddened the composite spectrum using the Galaxy, the LMC, and the SMC extinction curves (see Srianand et al. 2008; Noterdaeme et al. 2009, 2010a for the detailed procedure). These extinction curves differ significantly only at $\lambda < 2500 \text{ \AA}$. For J1443+0214, the SMC extinction curve is favored by the ultraviolet photometric points from the GALEX images. The J1443+0214 SED, along with the composite QSO SED reddened using the SMC extinction curve at $z_{\text{gal}} = 0.3714$ with the best fit $A_V = 0.61$, is shown in Fig. 5. We went on to apply the same procedure to a control sample of 223 SDSS-

II QSOs from Schneider et al. (2010) with emission redshifts within $\Delta z = \pm 0.005$ from that of J1443+0214, where we removed QSOs with strong BAL activity using Allen et al. (2011). We estimated the uncertainty due to intrinsic shape variations from the width of A_V distribution and corrected for the “zero-point” (the median A_V value). The extinction we thus derive for J1443+0214 is $A_V = 0.6 \pm 0.2$, i.e., 3σ evidence of reddening along the sight line when compared to the control sample. Since we did not attempt to remove intervening absorbers from the control sample, the estimated A_V and its statistical significance are conservative.

Next we use the Balmer decrement to obtain an independent estimate of the extinction. Various emission line fluxes estimated through the Gaussian profile fitting using a higher signal-to-noise ratio DR9 spectrum (Pâris et al. 2012) are given in Table 2. As noted above, different extinction curves are identical over the wavelength range of emission lines considered here and therefore yield similar values. From the observed Balmer decrement, we estimate the color excess $E(B-V) = E(H\beta - H\alpha)/(k(H\beta) - k(H\alpha)) \approx 0.19$ and 0.20 assuming intrinsic $H\alpha/H\beta = 2.86$ and $k(\lambda)$ for the SMC- and the Galaxy-type dust respectively (Gordon et al. 2003). This corresponds to $A_V = 0.6$ for $R_V = 2.74$ seen in the SMC. The extinction detected towards the QSO is significantly higher than the value ($E(B-V) < 0.03$) generally seen towards intervening DLAs and Mg II systems (e.g., York et al. 2006; Khare et al. 2012). It is also interesting to note that the extinction derived in the star-forming region using emission lines is remarkably consistent with the value derived along the QSO line of sight using SED fitting. This suggests that the abundance of dust is homogeneous over the length scale corresponding to the impact parameter (~ 5 kpc), over which the line fluxes are measured. Using the mean A_V vs $N(\text{H I})$ relationship found for the SMC (Gordon et al. 2003), we infer $N(\text{H I}) = (8 \pm 3) \times 10^{21} \text{ cm}^{-2}$.

Table 2. Emission line properties from the $z_{\text{gal}} = 0.3714$ galaxy towards J1443+0214

Line	F_{obs} ($10^{-17} \text{ erg s}^{-1} \text{ cm}^{-2}$)	$L^{(a)}$ ($10^{40} \text{ erg s}^{-1}$)	Derived quantities
[O II]	11.7	12.5	$\text{SFR} = 0.8 \text{ M}_{\odot} \text{ yr}^{-1(b)}$
[O III] $\lambda 5007$	24.8	21.4	$R_{23} = 13.8$
$H\beta$	3.4	3.0	$E(B-V) = 0.20$
$H\alpha$	12.1	8.5	$\text{SFR} = 0.7 \text{ M}_{\odot} \text{ yr}^{-1(c)}$

Notes. ^(a) Luminosity corrected for dust extinction ^(b) $L_{[\text{O III}]}$ - SFR calibration from Kewley et al. (2004). ^(c) $L_{H\alpha}$ - SFR calibration from Kennicutt (1998).

The profile of the 21-cm absorption line detected towards J1443+0214 is relatively simple (Fig. 2). In addition to a narrow component that can be modeled with a Gaussian of $\text{FWHM} \sim 8 \text{ km s}^{-1}$ ($T_K < 1400 \text{ K}$), a broad component is also required to reasonably fit absorption in wings (Table 1). The total integrated 21-cm optical depth corresponds to $N(\text{H I}) = 6.2 \times 10^{20} (T_s/100)(1.0/f_c) \text{ cm}^{-2}$, which is less than the $N(\text{H I})$ we inferred from the SED fitting. This could either be due to the covering factor of the gas being much less than 1 or the harmonic mean T_s being as high as $\sim 1400 \text{ K}$. No mas-scale images or $N(\text{H I})$ measurements using $\text{Ly}\alpha$ are available to distinguish between these scenarios. Another possibility is that the extinction per hydrogen atom in this absorber is much higher than what is measured in the SMC. It has been suggested that this may be the case in some high- z dusty Mg II absorbers with

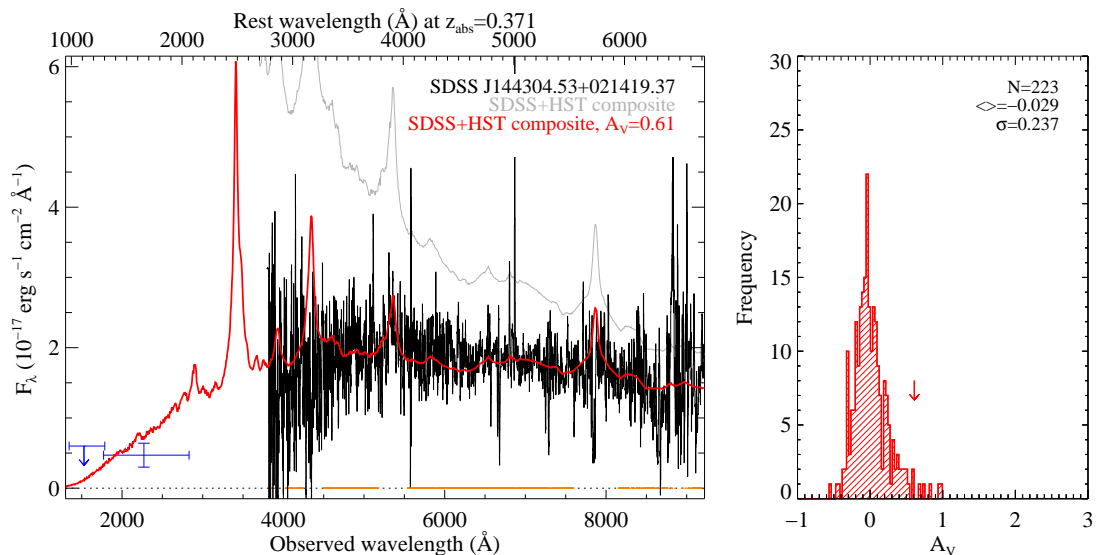


Fig. 5. *Left:* The SDSS spectrum of J1443+0214 (black) compared with the unreddened QSO composite (grey) and matched with the same QSO composite with SMC-extinction law at $z_{\text{gal}} = 0.3714$ and $A_V = 0.61$ (red). In the ultraviolet range (points with error bars), we use the photometric data from GALEX to estimate the flux. The orange segments at $y=0$ indicate the spectral range considered in the fitting process. *Right:* The distribution of A_V using SMC extinction law for a control sample of QSOs. The number of QSOs (N), the median ($\langle \rangle$), and rms (σ) A_V are also provided (see text for details). The arrow indicates the position of QSO J1443+0214.

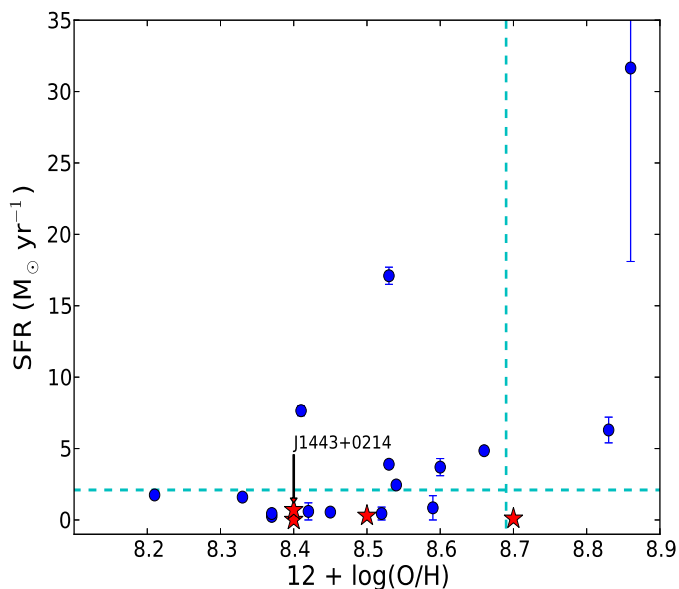


Fig. 6. Star formation rate versus metallicity for galaxies with 21-cm absorption ($z_{\text{gal}} < 0.4$; stars) and [O III]-emitting galaxies ($0.4 < z_{\text{gal}} < 0.8$; circles) from Noterdaeme et al. (2010b). The horizontal dashed line marks the median SFR for [O III]-emitting galaxies. The vertical dashed line corresponds to solar abundance, $12 + \log(\text{O}/\text{H})_{\odot} = 8.69$ (Asplund et al. 2009).

21-cm absorption (Gupta et al. 2012) and DLAs with CO detections (Noterdaeme et al. 2010a).

Now we use nebular emission line properties to obtain insight into the nature of the absorbing galaxy. We correct emission line fluxes for extinction and use these to estimate the global metallicity and star formation rate (SFR) of the galaxy (Table 2). For J1443+0214 we estimate the R_{23} ratio, defined

as $([\text{O II}] + [\text{O III}])/\text{H}\beta$, to be 13.8. In general, the R_{23} calibration is double-valued with respect to metallicity, and additional line ratios are required to break this degeneracy. For J1443+0214, the measured ratio is a high value at the turnover of the high- and low-metallicity branches of R_{23} -metallicity calibration (see e.g., Kobulnicky et al. 1999; Pilyugin 2000), indicating $12 + \log(\text{O}/\text{H}) \sim 8.4$ i.e., $0.5Z_{\odot}$ using $12 + \log(\text{O}/\text{H})_{\odot} = 8.69$ (Asplund et al. 2009). From extinction-corrected $\text{H}\alpha$ luminosity, $L(\text{H}\alpha)$, and using the following relation from Kennicutt (1998),

$$\text{SFR}(\text{M}_{\odot} \text{yr}^{-1}) = 7.9 \times 10^{-42} L(\text{H}\alpha) (\text{ergs s}^{-1}), \quad (2)$$

we derive $\text{SFR} \sim 0.7 \text{M}_{\odot} \text{yr}^{-1}$. Using the following relation from Kewley et al. (2004)

$$\text{SFR}(\text{M}_{\odot} \text{yr}^{-1}) = (6.6 \pm 1.7) \times 10^{-42} L([\text{O II}]) (\text{ergs s}^{-1}) \quad (3)$$

a similar value of $0.8 \pm 0.2 \text{M}_{\odot} \text{yr}^{-1}$ is derived using $L(\text{O II})$. Thus, the SFR is slightly below the median value, and the metallicity is well within the range of values found for such [O III]-emitting galaxies by Noterdaeme et al. (2010b) (see Fig. 6). In Fig. 6, the metallicity measurements for galaxies detected by Noterdaeme et al. (2010b) correspond to the upper branch of R_{23} -metallicity calibration. The corresponding metallicities on the lower R_{23} branch would be typically 0.4 dex lower. The SFRs for these have been estimated using calibrations (Eqs. 23 and 24) from Argence & Lamareille (2009) that use uncorrected [O II] and $\text{H}\beta$ luminosities. The error bars in Fig. 6 indicate the range of SFRs allowed by variations in dust attenuation and metallicity but do not account for fiber losses.

In addition to QGP J1443+0214, galactic emission lines superimposed on top of QSO continuum in SDSS fiber (diameter $3''$) spectra have been detected for three other 21-cm absorbers. For these four absorbers, we are able to obtain SFR, SFR per unit area (Σ_{SFR}) and metallicity (see Table 3 and references given in the last column for details). The SFR and metallicity

Table 3. Emission line properties of 21-cm absorbers/DLAs

Quasar	z_{qso}	Galaxy	z_{gal}	b (kpc)	$\int \tau dv$ (km s^{-1})	$12+\log(\text{O}/\text{H})$	$[\text{O}/\text{H}]^{(a)}$	SFR ($M_{\odot} \text{ yr}^{-1}$)	$\Sigma_{\text{SFR}}^{(b)}$	Reference
J104257+074850	2.7	J104257+074751	0.03	1.7	0.2	8.4	-0.29	0.01	4.1	Borthakur et al. (2010)
J124157+633241	2.6	J124157+633237	0.14	11	2.9	8.7	0.01	0.1	2.9	Gupta et al. (2010)
J144304+021419	1.8	–	0.37	<5	3.4	8.4	0.29	0.7	>3.8	This work
J163956+112758	1.0	J163956+112802	0.08	4.0	15.7	8.5	-0.19	0.3	18	Srianand et al. (2013)

Notes. ^(a) $[\text{O}/\text{H}] = \log(\text{O}/\text{H}) - \log(\text{O}/\text{H})_{\odot}$ ^(b) in units of $10^{-3} M_{\odot} \text{ yr}^{-1} \text{ kpc}^{-2}$

for these 21-cm absorbers are also plotted in Fig. 6 for comparison with the sample of [O III]-selected normal galaxies of Noterdaeme et al. (2010b). Figure 6 suggests that the SFR of 21-cm absorbers is less than the median SFR of [O III]-selected Mg II absorbers. While in the case of J1443+0214 we are sure that all the galactic emission is included in the SDSS fiber, in other cases a large fraction of foreground galaxy emission falls outside the SDSS fiber. Therefore, SFRs for these galaxies are at best lower limits, and are in general underestimated with respect to the higher redshift ($0.4 < z_{\text{gal}} < 0.7$) sample of Noterdaeme et al. (2010b). Therefore, within uncertainties SFRs for these QGPs with 21-cm absorption seem to be consistent with [O III]-selected Mg II absorbers.

4. Discussion

We have detected 21-cm absorption from two foreground galaxies at $z \sim 0.3$ towards quasars J0849+5108 ($b \sim 14$ kpc) and J1443+0214 ($b < 5$ kpc). In both cases, we infer $N(\text{H I}) \gtrsim 2 \times 10^{20} \text{ cm}^{-2}$, which qualifies these systems as DLAs. The integrated 21-cm optical depths are 0.95 km s^{-1} for J0849+5108 and 3.4 km s^{-1} for J1443+0214. As can be noted from Fig. 19 of Gupta et al. (2010), such high values are observed among $z < 1$ DLAs with host galaxy located at $b < 15$ kpc. In the case of J0849+5108, the SDSS photometry suggests that the Na I, Ca II, and 21-cm absorption lines detected by us are associated with an LRG having a smooth optical morphology that is typical of a passively evolving early-type galaxy. In the case of J1443+0214, the absorption is probably associated with a low surface brightness (LSB) galaxy identified via optical emission lines within ~ 5 kpc of the QSO sight line. Late-type or LSB galaxies have been identified with a few low- z DLAs and 21-cm absorbers (see Table 4 of Rao et al. 2003; Le Brun et al. 1997). However, the case of LRG associated with the absorber towards J0849+5108 is the first example of an early-type galaxy associated with an intervening 21-cm absorber. The gas detected in 21-cm and metal absorption lines in the outskirts ($b \sim 14$ kpc) of this LRG could be associated with the extended H I disks ($N(\text{H I}) \sim 10^{20} \text{ cm}^{-2}$) detected in deep H I 21-cm emission observations of local early-type galaxies (e.g., Serra et al. 2012). In particular, the cold gas detected in 21-cm absorption could be serving as fuel to the renewed star formation activity in the outer regions of the galaxy. This idea is supported by detections of ultraviolet rings that correspond to extended low-level recent or ongoing star formation in outskirts of $z \sim 0.1$ early-type galaxies (Salim et al. 2012; Fang et al. 2012).

DLAs, as well as 21-cm absorption line surveys at $z < 2$, are generally based on QSO sight lines selected via Mg II absorption (Rao et al. 2006), and it is well known that LRGs offer very little cross-section to Mg II absorption (Bowen & Chelouche 2011).

Indeed, in an Mg II selected sample of DLAs, sub-DLAs and Lyman limit systems at $0.1 < z < 1.0$ Rao et al. (2011) find that absorber galaxies comprise a mix of spectral types that are predominantly late type. Of eight DLA galaxies in the part of their sample with sufficient photometry to carry out galaxy template fits, only one is found to be early type. Clearly, much larger samples are required to quantify the prevalence of early-type galaxies in samples of DLA and 21-cm absorber hosts. The techniques that rely solely on the detection of nebular emission lines to identify absorber hosts may miss such cases.

Now we turn to low- z 21-cm absorbers with detections of nebular emission lines in QSO spectra. The SFR of absorbing galaxy in the case of J1443+0214 presented here is well below the median SFR found for [O III]-selected Mg II absorbers at $0.4 < z < 0.7$ (Noterdaeme et al. 2010b). A large fraction (87%) of these [O III]-selected absorbers exhibits strong Mg II absorption ($W_{\text{r}} > 1 \text{ \AA}$). This, along with the detection of strong Fe II absorption in several cases, suggests that most of these systems could be DLAs (see Rao et al. 2006). Wolfe et al. (2003) have used C II* to infer Σ_{SFR} in $z > 2$ DLAs. For the CNM-model i.e. where QSO sight lines pass through CNM, they measure $\Sigma_{\text{SFR}} = 10^{-2.2} M_{\odot} \text{ yr}^{-1} \text{ kpc}^{-2}$ and measure $\Sigma_{\text{SFR}} = 10^{-1.3} M_{\odot} \text{ yr}^{-1} \text{ kpc}^{-2}$ for the warm neutral medium (WNM)-model. The Σ_{SFR} that we measure for low- z QGPs in Table 3 are more in line with the CNM-model. This is not surprising since the presence of CNM in these cases is confirmed by the detection of 21-cm absorption. The abundances we infer for these QGPs using emission lines are in the range, $[\text{O}/\text{H}] \sim -0.3$ to 0.3 (Table 3), and are significantly higher than the values generally inferred for $z > 2$ DLAs using absorption lines. It will be interesting to obtain ultraviolet spectra of these QGPs to measure $N(\text{H I})$ and metallicity. This will also provide a direct measurement of spin temperature and CNM fraction along the sight lines, and will be crucial for understanding low CNM fractions in $z > 2$ DLAs inferred from the observations of 21-cm and H₂ absorption (e.g., Kanekar & Chengalur 2003; Srianand et al. 2012).

At $z > 2$, where it is possible to build large samples of DLAs via ground-based optical surveys (Noterdaeme et al. 2012b), searches to detect DLA host galaxies have mostly resulted in non-detections (e.g., Moller & Warren 1993; Rahmani et al. 2010). Recently, thanks to powerful instrumentation on the VLT, detections of a few DLA host galaxies have been possible by specifically targeting high-metallicity/ $N(\text{H I})$ DLAs (see e.g., Fynbo et al. 2011; Noterdaeme et al. 2012a). Using a sample of ten DLA hosts at $z > 2$, Krogager et al. (2012) report anti-correlation (Spearman rank, $r_s = -0.6$) between $\log N(\text{H I})$ and the galaxy impact parameter (see also Péroux et al. 2011). A similar trend is expected between 21-cm optical depth and impact parameter albeit with a large scatter probably due to further dependence on T_s and f_c . The strength of this correlation can po-

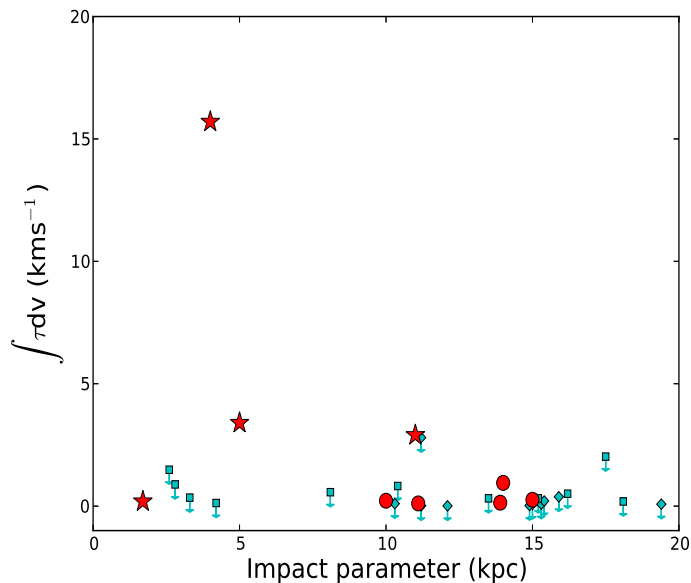


Fig. 7. Integrated 21-cm optical depth vs impact parameter for QGPs with 21-cm absorption measurements. The QGPs from Table 3 are plotted as stars. Also plotted as diamonds and squares are 3σ upper limits corresponding to a velocity resolution of 10 km s^{-1} from Tables 2 and 5 of Gupta et al. (2010) and Table 3 of Borthakur et al. (2011), respectively.

tentially shed light on processes driving the CNM filling factor of DLAs. In Fig. 7, we plot 21-cm optical depth versus impact parameter for all the $z \leq 0.4$ QGPs with 21-cm absorption measurements (Gupta et al. 2010; Borthakur et al. 2011). The Spearman rank correlation coefficient test suggests weak ($r_s = -0.3$) anti-correlation between $\int \tau dv$ and b for QGPs with 21-cm detection. Milliarcsecond scale images and 21-cm absorption spectra along with a much larger sample, especially with $b < 10 \text{ kpc}$, are required to confirm and understand the implication of this trend. Because the number of DLAs and consequently DLA hosts at $z > 2$ is expected to steadily increase with the availability of large samples of QSO spectra from the SDSS Baryon Oscillation Spectroscopic Survey (Noterdaeme et al. 2012b), all this clearly motivates the need for large surveys of 21-cm absorption line especially at low- z where it is relatively easy to identify and determine the properties of absorbing galaxy. Such surveys will become possible in the near future with SKA pathfinders and will uncover a new population of high- $N(\text{H I})$ absorbers i.e., DLA/sub-DLAs that have escaped optical/ultraviolet absorption line surveys due to biases caused by either dust extinction or pre-selection of QSO sight lines based on various metal absorption lines or on the proximity to a certain galaxy type.

Acknowledgments

We gratefully acknowledge V. Mohan's help with the subtraction of QSO contribution from SDSS images and useful discussions with P. Serra. We thank the GMRT staff for their help during the observations. GMRT is run by the National Centre for Radio Astrophysics of the Tata Institute of Fundamental Research. We acknowledge the use of SDSS spectra from the archive (<http://www.sdss.org/>). RS and PPJ gratefully acknowledge support from the Indo-French Centre for the Promotion of Advanced Research (Project N.4304-2).

References

- Allen, J. T., Hewett, P. C., Maddox, N., Richards, G. T., & Belokurov, V. 2011, *MNRAS*, 410, 860
- Argence, B. & Lamareille, F. 2009, *A&A*, 495, 759
- Arp, H., Sargent, W. L. W., Willis, A. G., & Oosterbaan, C. E. 1979, *ApJ*, 230, 68
- Asplund, M., Grevesse, N., Sauval, A. J., & Scott, P. 2009, *ARA&A*, 47, 481
- Boisse, P., Dickey, J. M., Kazes, I., & Bergeron, J. 1988, *A&A*, 191, 193
- Borthakur, S., Tripp, T. M., Yun, M. S., et al. 2011, *ApJ*, 727, 52
- Borthakur, S., Tripp, T. M., Yun, M. S., et al. 2010, *ApJ*, 713, 131
- Bowen, D. V. & Chelouche, D. 2011, *ApJ*, 727, 47
- Briggs, F. H. & Wolfe, A. M. 1983, *ApJ*, 268, 76
- Carilli, C. L. & van Gorkom, J. H. 1992, *ApJ*, 399, 373
- Curran, S. J., Tzanavaris, P., Darling, J. K., et al. 2010, *MNRAS*, 402, 35
- D'Ammando, F., Orienti, M., Finke, J., et al. 2012, *MNRAS*, 426, 317
- Darling, J., Macdonald, E. P., Haynes, M. P., & Giovanelli, R. 2011, *ApJ*, 742, 60
- Fang, J. J., Faber, S. M., Salim, S., Graves, G. J., & Rich, R. M. 2012, *ApJ*, 761, 23
- Ferlet, R., Vidal-Madjar, A., & Gry, C. 1985, *ApJ*, 298, 838
- Fynbo, J. P. U., Ledoux, C., Noterdaeme, P., et al. 2011, *MNRAS*, 413, 2481
- Gordon, K. D., Clayton, G. C., Misselt, K. A., Landolt, A. U., & Wolff, M. J. 2003, *ApJ*, 594, 279
- Gupta, N., Srianand, R., Bowen, D. V., York, D. G., & Wadadekar, Y. 2010, *MNRAS*, 408, 849
- Gupta, N., Srianand, R., Petitjean, P., et al. 2012, *A&A*, 544, A21
- Gupta, N., Srianand, R., Petitjean, P., Noterdaeme, P., & Saikia, D. J. 2009, *MNRAS*, 398, 201
- Heiles, C. & Troland, T. H. 2003, *ApJ*, 586, 1067
- Hopkins, A. M. & Beacom, J. F. 2006, *ApJ*, 651, 142
- Kanekar, N. & Chengalur, J. N. 2003, *A&A*, 399, 857
- Kanekar, N., Prochaska, J. X., Ellison, S. L., & Chengalur, J. N. 2009, *MNRAS*, 396, 385
- Kennicutt, Jr., R. C. 1998, *ARA&A*, 36, 189
- Kewley, L. J., Geller, M. J., & Jansen, R. A. 2004, *AJ*, 127, 2002
- Khare, P., vanden Berk, D., York, D. G., Lundgren, B., & Kulkarni, V. P. 2012, *MNRAS*, 419, 1028
- Kobulnicky, H. A., Kennicutt, Jr., R. C., & Pizagno, J. L. 1999, *ApJ*, 514, 544
- Krogager, J.-K., Fynbo, J. P. U., Møller, P., et al. 2012, *MNRAS*, 424, L1
- Lane, W. 2000, PhD thesis, University of Groningen
- Le Brun, V., Bergeron, J., Boisse, P., & Deharveng, J. M. 1997, *A&A*, 321, 733
- Møller, P. & Warren, S. J. 1993, *A&A*, 270, 43
- Noterdaeme, P., Laursen, P., Petitjean, P., et al. 2012a, *ArXiv e-prints*
- Noterdaeme, P., Ledoux, C., Srianand, R., Petitjean, P., & Lopez, S. 2009, *A&A*, 503, 765
- Noterdaeme, P., Petitjean, P., Carithers, W. C., et al. 2012b, *A&A*, 547, L1
- Noterdaeme, P., Petitjean, P., Ledoux, C., et al. 2010a, *A&A*, 523, A80+
- Noterdaeme, P., Srianand, R., & Mohan, V. 2010b, *MNRAS*, 403, 906
- Östman, L., Goobar, A., & Mörtzell, E. 2006, *A&A*, 450, 971
- Pâris, I., Petitjean, P., Aubourg, É., et al. 2012, *A&A*, 548, A66
- Péroux, C., Bouché, N., Kulkarni, V. P., York, D. G., & Vladilo, G. 2011, *MNRAS*, 410, 2237
- Pilyugin, L. S. 2000, *A&A*, 362, 325
- Rahmani, H., Srianand, R., Noterdaeme, P., & Petitjean, P. 2010, *MNRAS*, 409, L59
- Rao, S. M., Belfort-Mihalyi, M., Turnshek, D. A., et al. 2011, *MNRAS*, 416, 1215
- Rao, S. M., Nestor, D. B., Turnshek, D. A., et al. 2003, *ApJ*, 595, 94
- Rao, S. M., Turnshek, D. A., & Nestor, D. B. 2006, *ApJ*, 636, 610
- Salim, S., Fang, J. J., Rich, R. M., Faber, S. M., & Thilker, D. A. 2012, *ApJ*, 755, 105
- Schneider, D. P., Richards, G. T., Hall, P. B., et al. 2010, *AJ*, 139, 2360
- Serra, P., Oosterloo, T., Morganti, R., et al. 2012, *MNRAS*, 422, 1835
- Srianand, R., Gupta, N., Petitjean, P., et al. 2012, *MNRAS*, 421, 651
- Srianand, R., Gupta, N., Petitjean, P., Noterdaeme, P., & Saikia, D. J. 2008, *MNRAS*, 391, L69
- Srianand, R., Gupta, N., Rahmani, H., et al. 2013, *MNRAS*, 428, 2198
- Stickel, M., Fried, J. W., & Kuehr, H. 1989, *A&A*, 224, L27
- Telfer, R. C., Zheng, W., Kriss, G. A., & Davidsen, A. F. 2002, *ApJ*, 565, 773
- Vanden Berk, D. E., Richards, G. T., Bauer, A., et al. 2001, *AJ*, 122, 549
- Wakker, B. P. & Mathis, J. S. 2000, *ApJ*, 544, L107
- Wiklund, T. & Combes, F. 1995, *A&A*, 299, 382
- Wolfe, A. M., Prochaska, J. X., & Gawiser, E. 2003, *ApJ*, 593, 215
- Wolfire, M. G., McKee, C. F., Hollenbach, D., & Tielens, A. G. G. M. 2003, *ApJ*, 587, 278
- York, D. G., Khare, P., Vanden Berk, D., et al. 2006, *MNRAS*, 367, 945
- York, D. G., Straka, L. A., Bishof, M., et al. 2012, *MNRAS*, 423, 3692
- Yuan, W., Zhou, H. Y., Komossa, S., et al. 2008, *ApJ*, 685, 801